

Structural Characterization of Microscopic Defects in (111) AgBr Microcrystals: Correlation of Stacking Fault Defects to Twin Boundary Morphology

Samuel Chen, A. E. Taddei, S. Jagannathan, and M. G. Antoniadis

Imaging Materials and Media, Research & Development, Eastman Kodak Company, Rochester, New York

The introduction of iodide into (111) AgBr platelet crystals is known to induce the formation of structural defects, as well as enhance the photographic response of the resulting AgBrI. The incorporation of iodide, introduced uniformly during crystal growth, has been reported to form internal stacking faults, and more recently dislocation arrays. By using thermal processing to induce structural defects to regrow back into their matrix, it is possible to use this technique to probe specific defect characteristics, often at the microstructure level. In this article, we reported a detailed study of two iodide induced defects in (111) AgBrI crystals, using electron microscopy, to determine their location and structural characteristics, as well as to estimate their enthalpy of activation.

Journal of Imaging Science and Technology 45: 230–233 (2001)

Introduction

(111) AgBrI platelet crystals are widely used light sensing photographic material. By carefully controlling the incorporation kinetics, location, and concentration of iodide (I^-) in the AgBr lattice, varying degrees of photo-response enhancements can be induced. There exists a considerable effort in managing the incorporated I^- of this material. When its concentration exceeds 3 mol %, structural defects can form in the resulting AgBrI, and transmission electron microscopy (TEM) is capable of detecting the presence of defects, such as stacking fault in this material.^{1,2} Due to its resolving power, TEM has been used extensively to probe and to test proposals for the nature and location of this defect.³ More recently, microscopy results have revealed the existence of a second type of structural defect, and preliminary evidence suggests the possibility of iodide induced charge density states near the surface of (111) AgBrI.⁴ To better resolve the nature of these defects, we have attempted to use thermal processing techniques in order to carefully control the appearance and disappearance of these structural perturbations. Here we report the results of such a designed study that can separate out these two intertwined features. In the process, it has been possible not only to ascertain their location and morphology, but also to estimate their enthalpy energy of activation.

Experimental

AgBrI Platelet Preparation

High aspect ratio AgBr/AgBrI (core/shell) platelets were grown in aqueous gelatin solution by first nucleating a

pure AgBr core at 35°C via the addition of AgNO₃ to approximately 0.1 M solution of NaBr containing ~0.2% bone gelatin. Subsequently, an AgBr_{0.88}I_{0.12} shell was precipitated onto the pure AgBr core after raising the temperature to 75°C, adjusting the gelatin concentration to 0.6%, and adding AgNO₃, NaBr and KI solutions at a controlled pAg ($-\log[Ag^+]$) of 8.8. At the end of the growth step, the suspension was cooled to 40°C, washed and filtered. The final pH was adjusted to ~5.5 and the pAg to about 8.3. The resultant platelets were found to have an equivalent circular diameter of ~1.2 μ m, and a thickness of ~0.1 μ m.

Transmission Electron Microscopy Analysis

For plan-view studies, the crystal suspension was diluted and directly deposited onto carbon coated TEM Cu grids. For cross section analysis, the platelet suspension was coated onto an acetate film support with additional gelatin, the resulting film trimmed, and then cryomicrotomed after cooling to about -110°C. The thin sections (~50 nm thick) were collected and floated off onto holey carbon films supported on Mo grids. All TEM observations were carried out using a liquid nitrogen cooled holder at a temperature of about -180°C, and high resolution lattice images were taken at 200 kV (JEM-2000 FX). The combination of {111} and {002} lattice fringes in the image was sufficient to reveal the orientation relationship of specific planes in the vicinity of the defects in the AgBrI platelets.

Emulsion Annealing

AgBrI platelets were annealed inside the TEM (~10⁻⁸ torr) using a high temperature sample holder (Gatan Model 628 Heating Holder). For plan-view studies, the AgBrI on Cu grid was placed inside the TEM, and then resistively heated within the sample cavity of the heating holder. For cross section studies, thin sections on Mo grids were similarly heat treated under vacuum in

Original manuscript received November 9, 2000

©2001, IS&T—The Society for Imaging Science and Technology

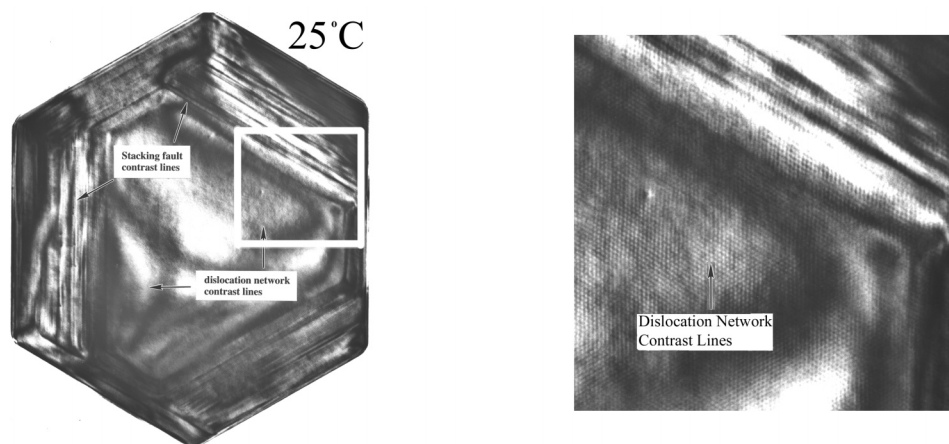


Figure 1. Unannealed $\text{AgBr}_{0.88}\text{I}_{0.12}$, showing diffraction contrast from stacking faults and dislocation networks.

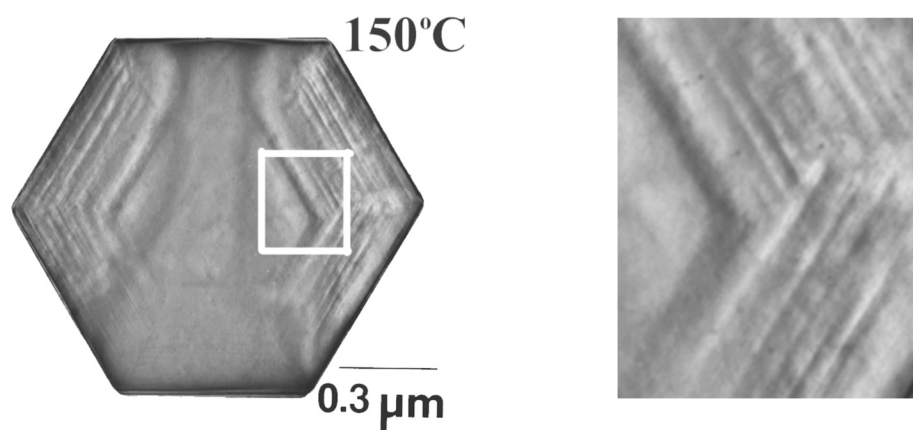


Figure 2. 150°C annealed $\text{AgBr}_{0.88}\text{I}_{0.12}$.

the TEM. After annealing, these grids were transferred to the cooling holder for observation.

Results and Discussions

Structural characteristics of iodide induced defects were first determined from plan-view observations. Unannealed platelets, when imaged under $(-2\ 2\ 0)$ two-beam bright field condition, are seen to contain two types of defects (Fig. 1). The first is associated with the shell, or higher iodide-containing region. This defect exhibits striation-like contrast and has previously been identified as stacking faults.^{1,3} These fringes run parallel to the platelet edges and have irregular spacings that are $\sim 0.01 - 0.03\ \mu\text{m}$ apart. The second, identified as dislocation networks, consists of three sets of closely spaced fringes (spacing $\sim 0.007\ \mu\text{m}$), that criss-cross each other at 120° , giving a grid-like pattern. These are seen over both the AgBr core and the AgBrI shell regions. When imaged under the $(-2\ 2\ 0)$ two-beam condition, the dot product of these defects' Burgers vector with the imaging beam vector becomes zero, i.e., under this condition, one of the three sets of stacking faults and dislocation

networks exhibits an invisibility criteria. Therefore, the Burgers vector of both defects is consistent with a value of $a/6\ [1\ 1\ -2]$, as pointed out previously.^{1,3}

Upon annealing at various temperatures between 25 and 225°C (up to 30 min), the two defects were found to anneal away at different temperatures. Between 140 and 150°C , contrast from the grid-like dislocation networks disappeared (Fig. 2), while the fringes from the stacking faults were removed after annealing at a higher temperature, 200°C (Fig. 3). We noted no sample decomposition at heating temperatures up to 225°C , except for occasional small specks of Ag islands on the platelet crystals, e.g., see arrowed feature in Fig. 3. Clearly, the observed difference in these annealing characteristics indicates the existence of two structural defects.

However, the location of these two defects within the crystal is difficult to assign based solely on image and Burgers vector analysis near the $\langle 111 \rangle$ zone axis. Hence, an effort was made to use cross sections to pinpoint their positions. Using cryo-microtomed thin sections, core/shell crystals were imaged after tilting to the $[1\ -1\ 0]$ axis orientation. Using an objective aperture to pass the $\{1\ 1\ -1\}$ and $\{0\ 0\ 2\}$ sets of diffracted beams, aligned high-resolu-

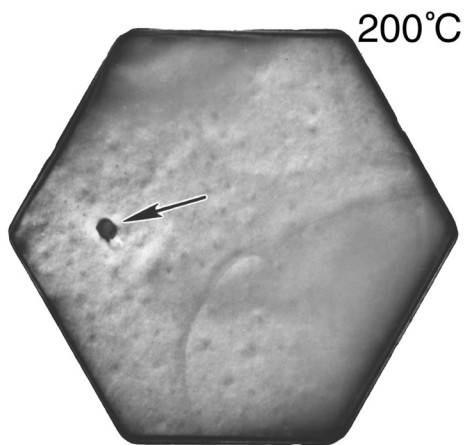


Figure 3. 200°C annealed $\text{AgBr}_{0.88}\text{I}_{0.12}$.

tion images were captured to reveal the location of the AgBrI lattice lines. For the unannealed crystals, the lattice images showed a high density of structural perturbation on the twin boundaries (Fig. 4). Otherwise, no structural defects with an occurrence density corresponding to the density of stacking faults or dislocation networks, visible in plan-view images, could be found.

Closer examination of the twin boundary regions revealed two types of structural perturbations. First, multiply-twinned segments, with varying thickness, lying parallel to the (111) twin boundaries were evident (Fig. 5). They occurred at irregular intervals, approximately $0.02\text{ }\mu\text{m}$ apart on the average, and were confined to the outer, lateral regions of microtomed sections. Second, especially evident in regions devoid of multiply-twinned segments, closely spaced jogs/steps segmenting the twin boundaries were seen. These jogs occurred in high frequency, and with irregularity, but on the average, they were separate from each other by about $0.007\text{ }\mu\text{m}$ (Fig. 6). These were found in the central region of microtomed sections. Using small diameter focused electron probes ($\sim 20\text{ nm}$), composition analysis of the twin boundary regions indicated that the area containing multiply-twinned segments is $\text{AgBr}_{0.88}\text{I}_{0.12}$, while that containing a high frequency of jogs is AgBr , consistent with their locations relative to the core/shell crystal architecture.

Upon annealing at 200°C under 10^{-8} Torr pressure, the microtomed films were found to have remained intact, with no discernible decomposition. Examination of the platelet cross-sections, under aligned $[1\text{ }-1\text{ }0]$ orientation to view the twin boundaries edge-on, revealed a significant finding. The twin boundaries of all the platelets appeared straight and uniform (Fig. 7). Clearly, the “segmented” morphology seen in the unannealed cross sections has been removed, i.e., annealing has induced both structural defects to regrow back into the AgBr face-centered-cubic matrix.

Therefore, correlation of plan-view to cross section data suggests that the stacking faults fringes correspond to thick multiply-twinned segments on the twin boundaries, while the grid-like network pattern correspond to a high density of dislocation jogs, also on the twin boundaries. This interpretation is different than that proposed earlier.^{1,4} Annealing at 200°C removes both the stacking faults and dislocation networks on the twin boundaries, causing these internal (111) planes to become smooth and straight.



Figure 4. Cross section micrograph of unannealed $\text{AgBr}_{0.88}\text{I}_{0.12}$.

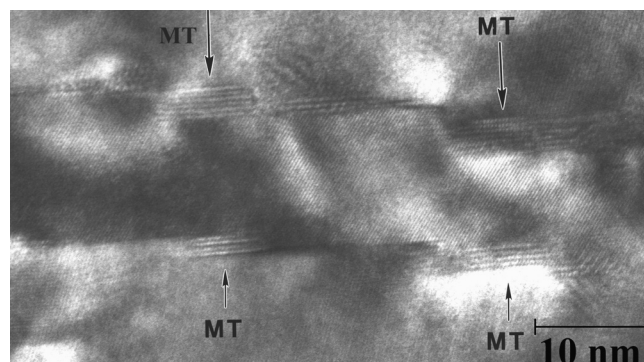


Figure 5. High-resolution image showing multiply twinned segments (MT) on the twin boundary in the high iodide shell portion of the unannealed $\text{AgBr}_{0.88}\text{I}_{0.12}$.

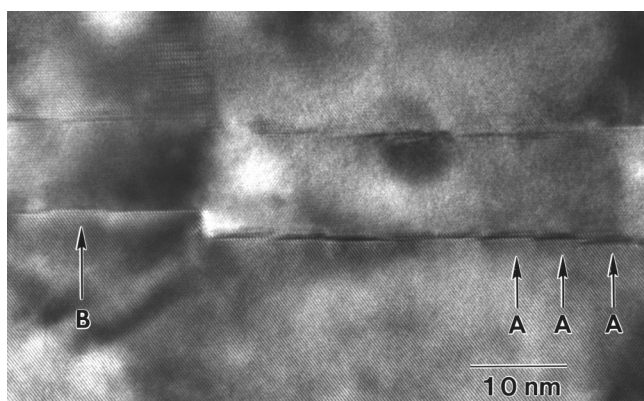


Figure 6. High-resolution image showing a high density of jogs (A and B) on the twin boundary of unannealed $\text{AgBr}_{0.88}\text{I}_{0.12}$.

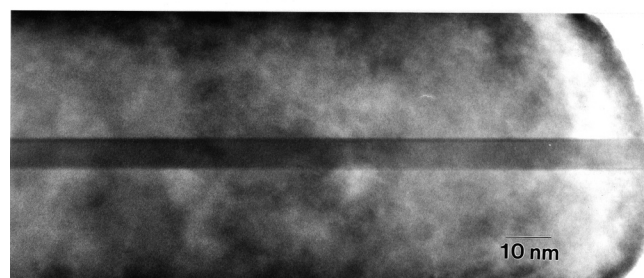
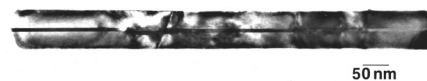


Figure 7. A low and a high magnification image showing the smooth and straight twin boundary morphology of a 200°C , annealed $\text{AgBr}_{0.88}\text{I}_{0.12}$.

These complimentary microstructure data suggests that the twin boundaries are sites where the incorporation of iodide can form multiply-twinned segments, in which the silver and halide ions are incorrectly positioned, relative to the regular face-centered-cubic AgBr lattice atom positions. This atomic stacking error is then manifested as small, localized stacking fault regions, which in turn causes the appearance of irregularly spaced striation-like contrast over the iodide rich shell region, in TEM plan-views. On the other hand, the high density of jogs on the twin boundaries, seen in cross section, represents a two-dimensional network of linear dislocation lines. Correspondingly, in plan-view, the parallel illumination of the electron beam should diffract off this internal defect network to form a grid-like pattern. The spacing between grid lines should be the average spacing of the dislocation network lines on the twin boundaries. Such grid-like patterns, caused by internal dislocation networks have been reported for other materials.^{5,6} Considering the location of the dislocation network defects over the pure AgBr core region, these necessarily are strain induced dislocations, caused by the deposition of lattice mismatched AgBrI over the (111) surface of AgBr core region.

It is possible to estimate the activation energy for annealing either dislocation networks or stacking faults given they anneal away in ~15 min at 150 and 200°C, respectively. Using the Arrhenius equation:

$$k = A e^{-E/RT} \quad (1)$$


and assuming $A = 4.1 \times 10^{12} \text{ s}^{-1}$ for AgBr⁷ and $k = 7.70 \times 10^{-4} \text{ sec}^{-1}$, as both defects have approximately the same reaction half-time, $t_{1/2}$ (~15 min), then,

$$\begin{aligned} E \text{ stacking fault} &= 34.9 \text{ kcal/mol, and} \\ E \text{ dislocation network} &= 30.8 \text{ kcal/mol} \end{aligned} \quad (2)$$

These calculations are presented here not as absolute values, but as a guide for future studies, especially for comparison between defects in AgX.

Results of these defect characteristics indicate the susceptibility of the (111) twin boundaries to form structural defects associated with uniform iodide incorporation during the growth of a high iodide shell region around a pure AgBr core. The formation of stacking faults and dislocations on the twin boundary presents some intriguing challenges for understanding how the lattice configuration of the twin boundary region can accommodate the incorporated iodide.

Summary

The complementary use of high-resolution electron microscopy coupled to the precise control of annealing temperatures has revealed the presence and location of two iodide induced defects in (111) AgBrI platelet crystals. These two structural perturbations are found to have similar defect core structures, and are both associated with deformation to the internal twin boundaries. Dislocation networks are found to anneal away by 150°C, while stacking faults regrow into the lattice at 200°C, under 10^{-8} torr pressure annealing conditions. The susceptibility of the (111) twin boundaries to form structural defects, associated with uniform iodide incorporation, is pointed out. 

References

1. C. Goessen, D. Schryvers, J. Van Landuyt, S. Amelinckx, A. Verbeeck, and R. De Keyser, *J. Crystal Growth* **110**, 930 (1991).
2. S. Urabe, U. S. Patent 4,879,208 (1989).
3. S. Chen, S. Jagannathan, R. V. Mehta, R. Jagannathan, and A. E. Taddei, *J. Imaging Sci. Technol.* **42**, 399 (1998).
4. C. Goessens, D. Schryvers, J. Van Landuyt, S. Amelinckx, and R. De Keyser, *Surf. Sci.* **337**, 153 (1995).
5. T. Y. Tan, S. L. Sass and R. W. Bulluffi, *Philos. Mag.* **31**, 575 (1975).
6. J. Spyridelis, P. Delavignette and S. Amelinckx, *Mat. Res. Bull.* **2**, 615 (1967).
7. C. R. A. Catlow, J. Corish, J. Harding, and P. W. M. Jacobs, *Philos. Mag.* **A55**, 481 (1987).